Research Paper

Design Sensitivity Studies on a Hydroacoustic Projector Using an Experimentally Validated Easy-to-Build Model

Vattaparambil Sreedharan SREEJITH⬤, Nachiketa TIWARI*⬤

Dhwani Laboratory, Department of Mechanical Engineering, Indian Institute of Technology Kanpur
Uttar Pradesh 208016, India; e-mail: vssree@iitk.ac.in
*Corresponding Author e-mail: ntiwari@iitk.ac.in

Hydroacoustic projectors are useful for generating low frequency sounds in water. Existing works on hydroacoustic projectors require two significant enhancements, especially for designers. First, we need to understand the influence of important projector design parameters on its performance. Such insights can be very useful in developing a compact and efficient projector. Second, there is a need for an integrated model of the projector based on easily available and user-friendly numerical tools which do not require development of complex customised mathematical analogs of projector components. The present work addresses both such needs. Towards these goals, an experimentally validated, easy-to-build projector model was developed and used to conduct design sensitivity studies. We show that reductions in pipe compliance and air content in oil, and an increase in orifice discharge coefficient can yield remarkable improvements in projector's SPL. We also show that reductions in pipe length and cylinder diameter cause moderate improvements in performance in mass and stiffness controlled regions, respectively. In contrast, the projector performance is insensitive to changes in pistonic mass, cylinder length, and diaphragm stiffness. Finally, we report that while pipe compliance and air content in oil can sharply alter system resonance, the effects of changes in pipe length and pistonic mass on it are moderate in nature.

Keywords: low frequency sound source; underwater transducer; fluid power; hydro-electro-mechano-acoustic analogy; hydraulic valve; piston; cylinder.

Nomenclature

A – area,
c – speed of sound,
C – capacitance,
C_d – coefficient of discharge,
$\overline{C_d}$ – average coefficient of discharge,
F – force,
F_f – Coulomb friction,
f – frequency,
k – stiffness,
l – length,
L – inductance,
m – mass,
p – pressure,
p_w – working pressure,
q – volumetric flow rate,
r – radius,
R – resistance,
R_m – viscous friction,

t – time,
t_p – thickness of the piston,
u – velocity,
V – volume,
V_f – volume fraction,
w – flow area gradient,
x – displacement,
Z – impedance.

Greek alphabet

β – bulk modulus,
γ – specific heat ratio,
μ – dynamic viscosity,
ρ – density,
ω – angular frequency.

Subscripts/Superscripts

AC – accumulator,
C – compliance effect,
cl – piston to cylinder radial clearance,

cy – hydraulic cylinder,
D – diaphragm,
H – hydraulic,
L – inertial effect,
m – mechanical,
p – piston,
r – radiation,
R – dissipative effect,
v – valve.

1. Introduction

Low frequency sound is widely used in several underwater applications. Amongst different types of low frequency projectors used to produce low frequency sound, hydroacoustic projectors have the best performance for a given size and mass (DUBUS *et al.*, 2013; DECARPIGNY *et al.*, 1991). While there is sufficient literature available on modelling of individual components of the projector, there are not many works (BOUYOUCOS, 1987; SREEJITH, TIWARI, 2016a; 2016b; 2020) describing a unified model for the entire system. Such a unified model can be developed either through use of bond graphs (BUSCH-VISHNIAC, PAYNTER, 1989), or by employing the lumped parameter approach (BAUER, 1954; SMITH, 1994; SCHÖNFELD, 1954; BERANEK, 1993) where mathematical equivalences between different operational domains are used to predict projector's behaviour. Amongst the latter, the work of SREEJITH and TIWARI (2020) offers a detailed methodology for developing an electrical analog of the projector. However, their work can be significantly enhanced in two ways, especially for designers. First, there is a need to develop insights regarding the influence of different design parameters on projector performance. Such insights can be very useful in developing a compact and an efficient hydroacoustic projector. Second, the unified model for the projector should use standard and easily available numerical tools. Such a modelling approach will not require significant efforts in developing customised mathematical analogs of components. The present work addresses both such needs.

In this work, we have used a MATLAB's Simscape Fluids$^{\text{TM}}$ (MATLAB, n.d.) based model of a hydroacoustic projector to conduct exhaustive design sensitivity studies related to eight important design parameters through more than 3000 simulations. These parameters include pipe compliance, air content in the oil, length of pipes, diameter and length of the cylinder, stiffness of the diaphragm, total pistonic mass, and orifice flow discharge coefficient. MATLAB's Simscape Fluids$^{\text{TM}}$ has been used earlier for modelling several hydraulic systems (SUI, LU, 2018; DING *et al.*, 2016; KIM *et al.*, 2012; PEA, LEAMY, 2015). However, it has never been used to model acoustic systems such as a hydroacoustic projector.

2. Modelling of the hydroacoustic projector

A hydroacoustic projector is made up of several pipelines, a bi-directional flow control valve, cylinder piston assembly, a diaphragm acting as a radiator, air behind diaphragm, and an accumulator. The working of such a projector has been discussed in detail in (SREEJITH, TIWARI, 2020) and is also explained in Appendix A. Our model developed in Simscape Fluids$^{\text{TM}}$ is shown in Fig. 1 and is described further.

Pipelines and working fluid: The pressure drop (Δp) across a short pipe due to viscous (Δp_R), inertial (Δp_L), and compressibility (Δp_C) effects is expressed as:

$$\Delta p(t) = \Delta p_R(t) + \Delta p_L(t) + \Delta p_C(t). \tag{1}$$

Mathematical relations for these pressure drops (AKERS *et al.*, 2006; MERRITT, 1967) are as follows:

$$\Delta p_R(t) = \frac{8\mu l}{\pi r^4} q(t) = R_H q(t), \tag{2}$$

$$q(t) = \frac{l\pi r^2}{\beta} \frac{\mathrm{d}p_C(t)}{\mathrm{d}t} = C_H \frac{\mathrm{d}p_C(t)}{\mathrm{d}t}, \tag{3}$$

$$\Delta p_L(t) = \frac{\rho l}{\pi r^2} \frac{\mathrm{d}q(t)}{\mathrm{d}t} = L_H \frac{\mathrm{d}q(t)}{\mathrm{d}t}. \tag{4}$$

As the standard pipe element in software does not account for Δp_L, an additional element (fluid inertia) was attached to each pipe element in series to account for it.

Next, properties of working fluid (density, bulk modulus, and viscosity) were defined in the custom hydraulic fluid element. To account for the presence of air, the effective bulk modulus of working fluid was adjusted based on the model proposed in (YANG *et al.*, 2011) using Eq. (5):

$$\beta_{\text{effective}} = \left(\beta_{\text{oil}}^{-1} + V_{f_{\text{air}}} \beta_{\text{air}}^{-1} \right)^{-1}. \tag{5}$$

Here β_{air} is the bulk modulus of air. It is the product of absolute working pressure (p_{pump}) and ratio of specific heats of air (γ_{air}).

Bi-directional control valve: It has been represented in our model by the 4-way directional valve element. Inputs to this element were maximum cross-sectional area of valve opening, flow discharge coefficient (C_d), and initial position of the spool. Since valve opening area varies with time, it was defined as a function through the valve excitation block. For an orifice of constant size, the relation between pressure and flow rate is given by Eq. (6) (LIU *et al.*, 2019; MERRITT, 1967; PAN *et al.*, 2011; WU *et al.*, 2003):

$$\Delta p = q \frac{q}{\left(C_d w_v x_v \sqrt{\frac{2}{\rho}} \right)^2} = q R_v. \tag{6}$$
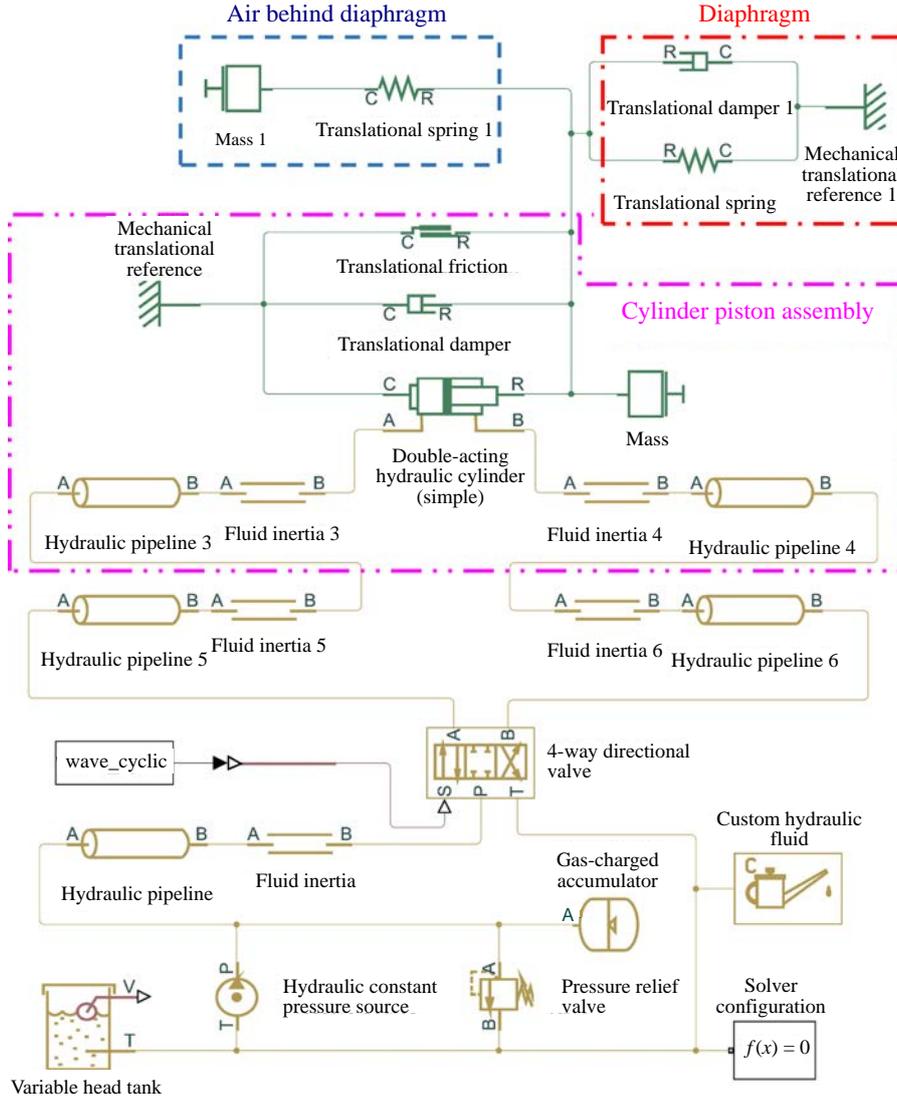
Fig. 1. Model developed in MATLAB Simscape Fluids$^{\text{TM}}$.

However, in this work the size of the orifice varies continuously, and thus the resistance offered by the opening is time dependent and a function of $q(t)$. For such orifices the relation between pressure and flow rate may be expressed as (SREEJITH, TIWARI, 2020):

$$\Delta p(t) = q(t) \frac{q(t)}{\left(\overline{C_d} w_v x_v(t) \sqrt{\frac{2}{\rho}}\right)^2} = q(t) R_v(t). \qquad (7)$$

Thus, in lieu of C_d, we provided the experimentally determined value of average coefficient of discharge $(\overline{C_d})$ as an input to the 4-way directional valve element.

Cylinder-piston assembly: The standard double-acting hydraulic cylinder block in Simscape Fluids$^{\text{TM}}$ formed the basis for representing cylinder-piston assembly in our model. Inputs to this block were piston area, piston stroke length, and initial location of the piston. However, such an element does not account for mass of the piston, fluid present on either sides of the

piston in the cylinder, and the friction between the piston and the cylinder. Thus, hydraulic pipelines 3 and 4, fluid inertia 3 and 4, mass, and translational friction elements were added to the double acting cylinder block to account for such effects. These details are shown in Fig. 1. It may be noted that the translational friction block accounts for Coulomb friction present between the piston and the cylinder. Inputs to this block, was the experimental value of peak force beyond which motion starts. Finally, viscous friction between the piston and the cylinder was also modelled through use of a transitional damping block. The force-velocity relations for such friction is given in Eq. (8). Thus, the input to this block was mechanical resistance (R_m):

$$F(t) = \frac{2\pi r_p t_p \mu}{r_{cl}} u(t) = R_m u(t). \qquad (8)$$

Diaphragm: The projector's diaphragm is made up of a moving mass and a suspension element. It also

sees radiation impedance from the surrounding media, which has an inductive component (related to moving mass of air) and a dissipative component. To account for these effects, the diaphragm block (see Fig. 1) was created. In this block, the experimentally determined stiffness of the diaphragm was represented through a translational spring. Also, the dissipative component of radiation impedance was modelled as a translational damper 1 with a value as defined in Eq. (9) (BERANEK, 1993):

$$R_r = \pi r_D^4 \rho_{\text{air}}\, \omega^2/(4c_{\text{air}}). \qquad (9)$$

Finally, the mass attributable to air loading was computed through Eq. (10) (BERANEK, 1993), and its value was added to the mass element in the cylinder-piston assembly block:

$$m_r = 2\omega r_D^3 \rho_{\text{air}}. \qquad (10)$$

Air behind diaphragm: There is a small volume of air behind the diaphragm which is connected to the atmosphere through a small air vent hole. These details are as shown in Fig. 6. The compliance of this air volume based on acoustic-mechanical analogy is $V_{\text{air}}/(\rho_{\text{air}} c_{\text{air}}^2 A_D^2)$ (SREEJITH, TIWARI, 2020). This value was used as an input to the translational spring 1 block. Further, the air in the small hole has some moving mass $(\rho_{\text{air}}\, l_{\text{hole}}/(A_{\text{hole}} A_D^2)$ (SREEJITH, TIWARI, 2020)). Here, l_{hole} and A_{hole} corresponds to the length and the cross-sectional area of the hole. This mass is represented as mass 1 in the model. Together, these two elements of the air behind diaphragm block are shown in Fig. 1.

Accumulator: A gas-charged accumulator block was used to model the accumulator of the hydroacoustic projector. The inputs to this accumulator were volume, pre-charge pressure, and specific heat ratio of the accumulator gas.

While developing the mathematical model of the hydroacoustic projector, we reviewed the results of several earlier works related to mathematical modelling of different projector components. Specifically, BAUER'S (1954) work on modelling of acoustical and mechanical components and the works of AKERS *et al.* (2006), MERRITT (1967), and SCHÖNFELD (1954) on mechanical and electrical equivalences of hydraulic elements were very useful. For modelling fluid flow in pipes, we referred to works of MIKOTA (2013), KRUS *et al.* (1994), LIN and HOLBERT (2009), and MATKO *et al.* (2000). Also results of LARSON and JÖNSSON (1991), CHO *et al.* (2000), AKKAYA (2006), RUAN and BURTON (2006), KARJALAINEN *et al.* (2012), and TOTTEN (2011) were useful in understanding the nature of influence of entrapped air, operating pressure, temperature, and pipe material on effective bulk modulus of the oil. To understand the role of friction between the hydraulic cylinder and the piston, work of HEINZE (2008) was helpful. Also the works of AKERS *et al.* (2006), MERRITT (1967), and BORUTZKY *et al.* (2002) were found useful in terms of understanding the nature of fluid flow through an orifice of a bi-directional valve. Finally, simulation models for hydraulic accumulators (EDGE, JOHNSTON, 1991; KAJASTE *et al.*, 2002; BARNWAL *et al.*, 2014; IJAS, 2007) were also very useful. The model developed in such a way was validated experimentally. The experimental setup for this was similar to the one used in (SREEJITH, TIWARI, 2020). For reader's convenience its details are provided in Appendix B.

3. Results and analysis

The mathematical model as described earlier was used to simulate projector performance for twelve test cases and validated against test data. Details of the test cases are shown in Table 1. While conducting these tests three parameters were varied. These were frequency of valve displacement (f), valve displacement amplitude ($x_{v_{\max}}$), and pressure produced by the pump (p_w). An important consideration during the selection of test parameters was that maximum operating frequency of the direction control valve was 2 Hz. Hence, most tests were conducted below 2 Hz. However, we also conducted some tests at 3, 5, and 10 Hz. While conducting experiments we noted that the motion of valve spool was periodic but not harmonic, even though the force excitation provided to the spool through the shaker was sinusoidal. We attribute such a phenomenon to the presence of friction between the spool and the valve block, and generation of pressure surges in the pipeline at valve closure time. Such effects could be minimised by using a more powerful electro-dynamic shaker and a better accumulator. To account for such phenomena in simulations we used measured displacement data of spool as an input to the model.

Table 1. Comparison of simulation and experiment data.

Test cases	f [Hz]	$x_{v_{\max}}$ [mm]	p_w [MPa]	$\overline{C_d}$
T_1	1	1.50	0.36	0.28
T_2	1	1.55	0.42	0.28
T_3	1.4	1.36	0.36	0.31
T_4	1.4	1.60	0.43	0.28
T_5	1.7	1.55	0.32	0.29
T_6	1.7	1.63	0.44	0.27
T_7	2	1.63	0.35	0.29
T_8	2	1.74	0.50	0.26
T_9	3	1.59	0.35	0.30
T_{10}	3	1.66	0.44	0.28
T_{11}	5	2.06	0.46	0.26
T_{12}	10	1.96	0.24	0.28

Figure 2 compares experimental and simulation results for steady state diaphragm displacement and its
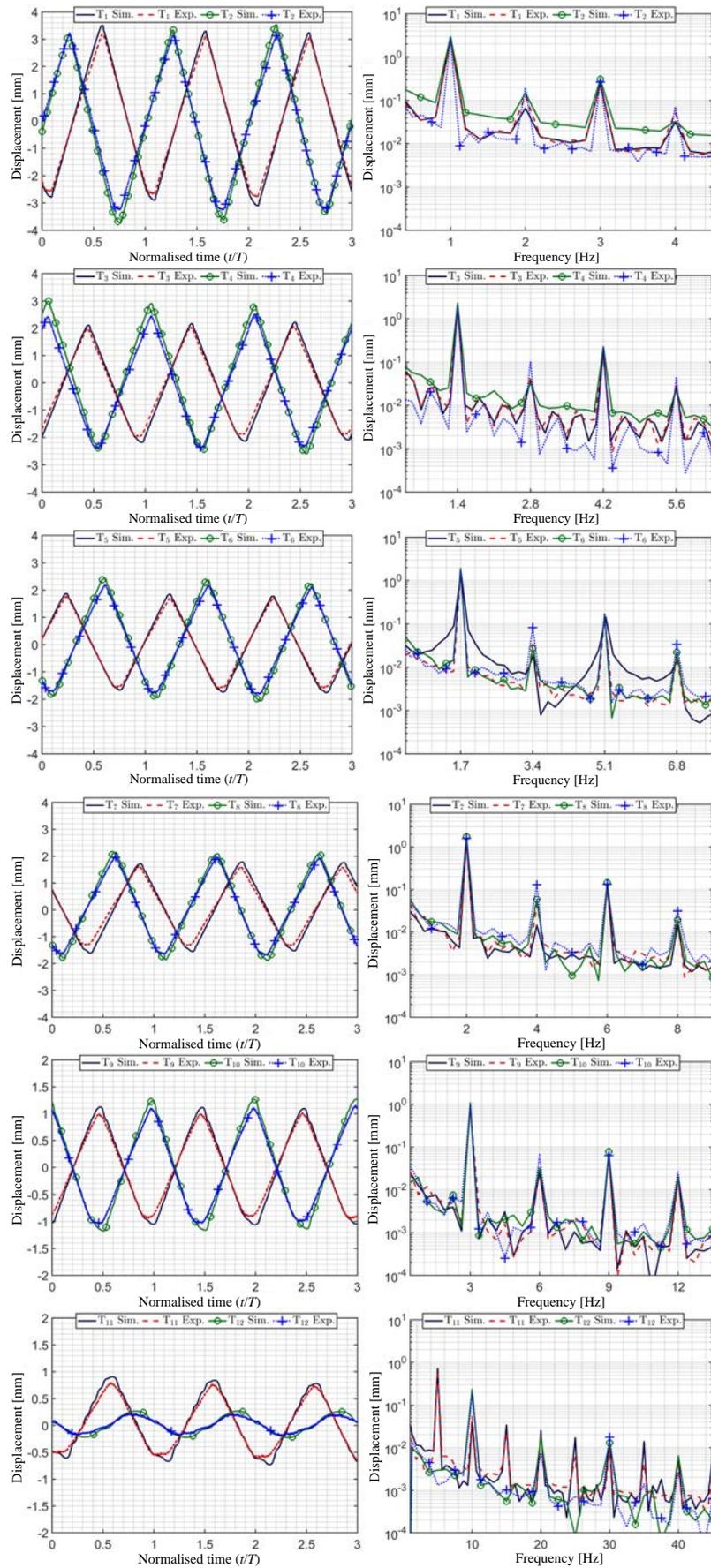
Fig. 2. Diaphragm displacement and spectra of diaphragm displacement from simulations and experiments.
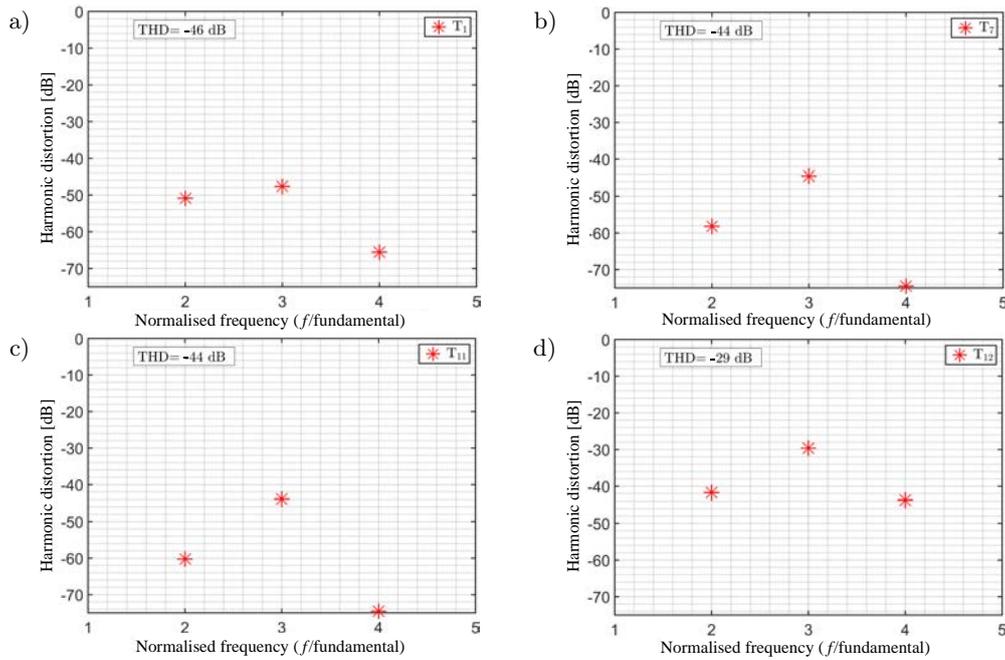
Fig. 3. Results from simulation on harmonic distortion in diaphragm displacement for cases T_1 (a), T_7 (b), T_{11} (c), and T_{12} (d) when valve spool displacement signal was purely harmonic.

FFT, respectively, for all test cases. Table 2 compares 1st harmonic amplitudes received from experiments and simulation for all test cases. These figures show that a good agreement exists between experimental and simulation results. It is also noted that the difference between numerical and experimental results somewhat increases at higher frequencies.

Table 2. Comparison of simulation and experiment data.

Test cases	Amplitude of 1st harmonic [mm]		Difference	
	Experiment	Simulation	%	dB
T_1	2.50	2.74	−8.6	−0.8
T_2	2.73	2.95	−7.7	−0.7
T_3	1.73	1.88	−8.1	−0.7
T_4	2.08	2.29	−9.4	−0.9
T_5	1.44	1.53	−6.4	−0.6
T_6	1.72	1.90	−9.9	−0.9
T_7	1.28	1.45	−12.2	−1.1
T_8	1.58	1.75	−9.7	−0.9
T_9	0.87	0.99	−11.8	−1.1
T_{10}	0.97	1.09	−11.5	−1.1
T_{11}	0.64	0.72	−11.3	−1.0
T_{12}	0.18	0.24	−25.1	−2.5

% = (experiment−simulation) × 100/(simulation)

dB = 20 log (experiment/simulation)

For the 12 test cases studied, we also explored the extent of distortion in terms of magnitudes of higher order harmonics generated by the projector had the valve spool displacement been truly harmonic. These studies were based on simulation only. Figure 3 shows that distortion introduced in the output, i.e. diaphragm displacement, is very small. Thus, we would expect the hydroacoustic projector to behave linearly across a range of frequencies.

Next, the performance of the hydroacoustic projector in terms of SL (source level) was calculated. The results from these exercises are presented in Fig. 4. In the figure, three sets of data are presented. The first two sets correspond to SL data based on experimental and simulation data for 12 test cases. The figure shows that good agreement exists between the experiments and simulations. The third set of data corresponds to SL expected from the projector based on simulations with valve displacement, where the inlet pressure was set at 1.4 mm and 0.4 MPa, respectively. This curve was used as the baseline while conducting design sensitivity studies for the projector.
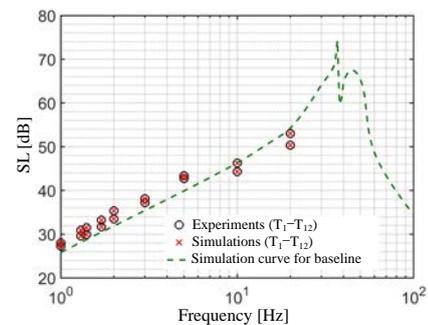
Fig. 4. SL produced by the projector.

3.1. Sensitivity studies

To learn the effects of different design parameters on projector performance, several sensitivity studies were conducted. Towards this, over 3000 simulations were conducted. Figure 5 shows detailed results from such studies. A detailed discussion of the same is provided further.

3.1.1. Effective orifice flow discharge coefficient

Figure 5 shows that the SL from the projector increases with increasing $\overline{C_d}$ at all frequencies except at resonance. This occurs because, as per Eq. (6), the flow rate through the valve (q) is directly proportional to $\sqrt{C_d}$. The value of $\overline{C_d}$ can be improved through careful selection of better valves, especially those
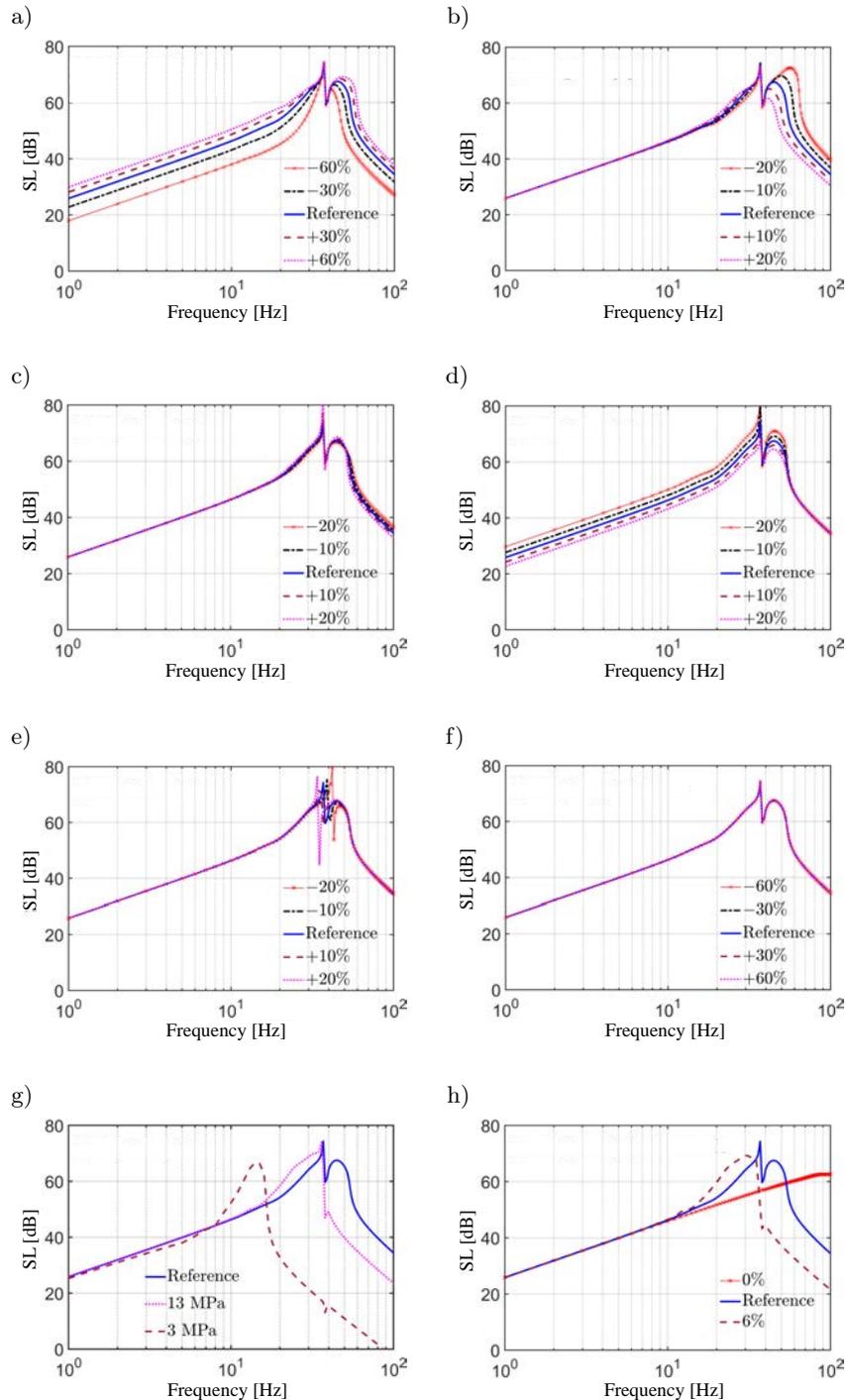
Fig. 5. Sensitivity of the device to different parameters: a) orifice flow discharge coefficient, b) length of pipe, c) cylinder length, d) cylinder diameter, e) pistonic mass, f) diaphragm stiffness, g) pipe compliance, h) oil compressibility due to presence of air.

which have wider openings, and a better spool profile. Since Eq. (6) also shows that q is directly proportional to w_v (valve spool land perimeter), a valve with larger w_v will also yield a higher SL.

3.1.2. Length of pipes

When the length of a pipe is reduced, hydraulic capacitance (C_H) and hydraulic inductance (L_H) decrease as per Eqs (3) and (4). Thus, the resonance frequency of the system value increases as it is inversely proportional to $\sqrt{L_H C_H}$. Such an increase is clearly reflected in Fig. 5. Further, because of such changes the overall SL level should increase and decrease in mass and stiffness controlled regions, respectively. These, are indeed the trends seen in Fig. 5. In the stiffness controlled region, SL decreases with a reduction in the pipe length because of increase in the stiffness. In the mass controlled region, SL increases due to reduction in the pipe length as inertial effects get reduced. A reduction in the pipe length also decreases dissipation (R_H), which leads to increased SL at resonance. Such a trend is also seen in Fig. 5.

3.1.3. Cylinder length

The effect of changes in length of the cylinder is very similar to that due to change in the pipe length. However, the magnitude of such effects is small in the former case. This is because the overall length of the pipe (2550 mm) is about 3.31 times that of the cylinder. The design is much more sensitive to fractional changes in length of the pipe vis-à-vis the same in the cylinder.

3.1.4. Cylinder diameter

Figure 5 shows that an increase in diameter of the cylinder does not alter the resonance frequency. Such insensitivity is attributable to the fact that the product of C_H and L_H remains unchanged when the cylinder diameter changes. The figure also shows that an increase in diameter corresponds to reduced SL, especially prior to resonance, i.e. in the stiffness controlled region. This occurs because mechanical stiffness attributable to C_H (i.e. A_{cy}^2/C_H)[1] increases with increasing diameter, thereby leading to a reduction in the flow rate and SL.

3.1.5. Pistonic mass

We define pistonic mass as the total mass of piston and diaphragm. It is seen that an increase in its value corresponds to a reduction in the first resonance frequency and *vice versa*. However, such a change does not alter the performance at other frequencies because the magnitude of the change is very small relative to the overall dynamic mass of the system, which also includes the mass of oil.

---

[1] A_{cy} is cross-sectional area of the cylinder.

3.1.6. Diaphragm stiffness

Figure 5 also shows that the effect of the diaphragm stiffness on projector performance is not significant. This is because the stiffness offered by oil inside the cylinder is an order of magnitude larger than that of the diaphragm.

3.1.7. Pipe compliance

The resonance frequency of the projector should expectedly decrease with a reduction in $\beta_{\text{effective}}$. A reduction in $\beta_{\text{effective}}$ should also lead to a lower SL because a large fraction of input energy gets locked due to cyclic compression and expansion of the working fluid and pipes. To explore such effects, design sensitivity studies involving change in pipe compliance were conducted. Amongst these, the baseline case involved rigid pipes as in reality pipes were made of 2.5 mm thick steel. For such a case, the value of $\beta_{\text{effective}}$ as per Eq. (5) works out to be 23 MPa. However, if reinforced rubber pipes are used in lieu of steel pipes, then Eq. (5) needs to be modified to account for pipe compliance. The modified equation as per (Sreejith, Tiwari, 2020; Akkaya, 2006) is given below:

$$\beta_{\text{effective}} = \left(\beta_{\text{oil}}^{-1} + \beta_{\text{pipe}}^{-1} + V_{f_{\text{air}}}\beta_{\text{air}}^{-1}\right)^{-1}. \qquad (11)$$

In such a case the value of $\beta_{\text{effective}}$ can drop to a mere 3 MPa (Sreejith, Tiwari, 2021), thereby causing a reduction in resonance frequency, and SL. Figure 5 indeed shows that projector SL can degrade significantly due to such a reduction in pipe stiffness.

3.1.8. Oil compressibility due to presence of air

As per Eq. (5), the value of $\beta_{\text{effective}}$ of oil can get dramatically reduced if air is present in oil even in small amounts. Figure 5 shows the effect of air content on projector performance through analysis of three cases: oil with no air, oil with 3% air (reference), and oil with 6% air. We see that resonance frequency shifts downwards with increasing air content. We also note that projector SL decreases sharply as air content in oil is increased. This occurs because $\beta_{\text{effective}}$ exhibits a strong reduction with increasing air content.

4. Conclusions

An easy to build model of a hydroacoustic projector has been developed and verified against experimental data. Such a model was used to conduct detailed sensitivity studies to understand the influence of eight design parameters on projector performance. These parameters are: orifice flow discharge coefficient, length of pipes, cylinder length and diameter, pistonic mass, diaphragm stiffness, pipe compliance, and oil compressibility due to presence of air. Our studies show that reductions in pipe compliance and air content in oil,

and an increase in orifice discharge coefficient can yield remarkable improvements in projector's sound pressure level. The study also shows that reductions in pipe length and cylinder diameter lead to moderate improvements in projector performance in mass and stiffness controlled regions, respectively. In contrast, the projector performance is more or less insensitive to changes in pistonic mass, cylinder length, and diaphragm stiffness. Finally, we report that while pipe compliance and oil compressibility can sharply influence system resonance, effects of changes in pipe length and pistonic mass on it are moderate in nature.

Going further, the proposed projector model can be further improved by accounting for stick-slip friction in cylinder-piston assembly, non-linearities in diaphragm stiffness and damping, influence of bends and cross-sectional changes in pipes, and temperature changes in oil. A good analytical model of the valve can also be used to improve the current projector model. Such work can also help in development of better valves which in turn, can enhance projector performance at higher frequencies and flow rates. On the experimental side, the behaviour of projector can be improved through use of a stronger actuation system for the spool.

Appendix A. Working of the device

Figure 6 is a schematic sketch of the hydroacoustic projector. The projector uses a low power electrodynamic shaker to control the position of the spool of a directional control valve. The spool's back and forth movement relative to its neutral position modulates the unidirectional flow of oil emanating from the high power pump to time dependent pulsating flow. Thus if the spool is harmonically excited through a shaker, then the pulsating flow of hydraulic oil causes the piston in the main cylinder to move back and forth as well. Since the piston is connected to a diaphragm, acoustic power gets radiated in the medium around the diaphragm.
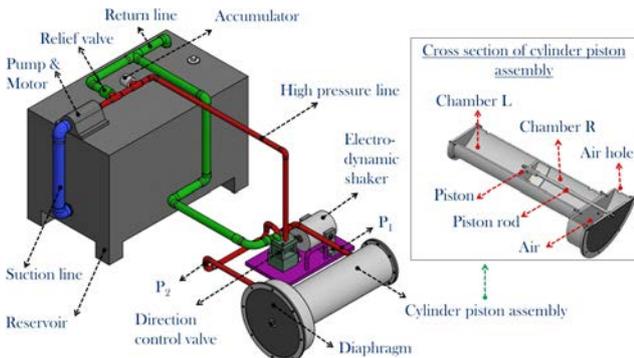
Fig. 6. Schematic of a hydroacoustic projector.

Next, we explain how exactly the unidirectional flow from pump gets modulated into pulsating flow.

For this, Fig. 7 provides details on the working of the direction control valve which has five external ports (A, B, C, D, and E). The valve also has four orifices O_1, O_2, O_3, and O_4 which when open connect Port A to D, A to E, E to C, and D to B, respectively. When, the valve spool is in neutral position all of its four orifices are closed and no oil flows through the system. However, if the spool moves rightwards of the neutral positions, high pressure oil from the pump flows from Port A to Port D via O_1 and then to the left (L) side of the hydraulic cylinder. Thus, the right (R) side of the hydraulic cylinder moves outwards and the oil exits from the main cylinder at low pressure and returns to the reservoir via path P_2-E-O_3. The overall direction of the flow reverses when the shaker drives the valve spool leftwards of the neutral position. In such a case the piston moves leftwards as well. In this half-cycle the oil flow path is A-O_2-II-E-P_2-R-L-P_1-D-I-O_4-B-reservoir. In this way, the periodic reversal of pressurised flow drives the diaphragm of sound projector back and forth, which in turn leads to radiation of sound into the external medium. The hydroacoustic projector also has an accumulator, which dampens out water hammer phenomenon caused due to sudden closure and opening of the direction control valve.
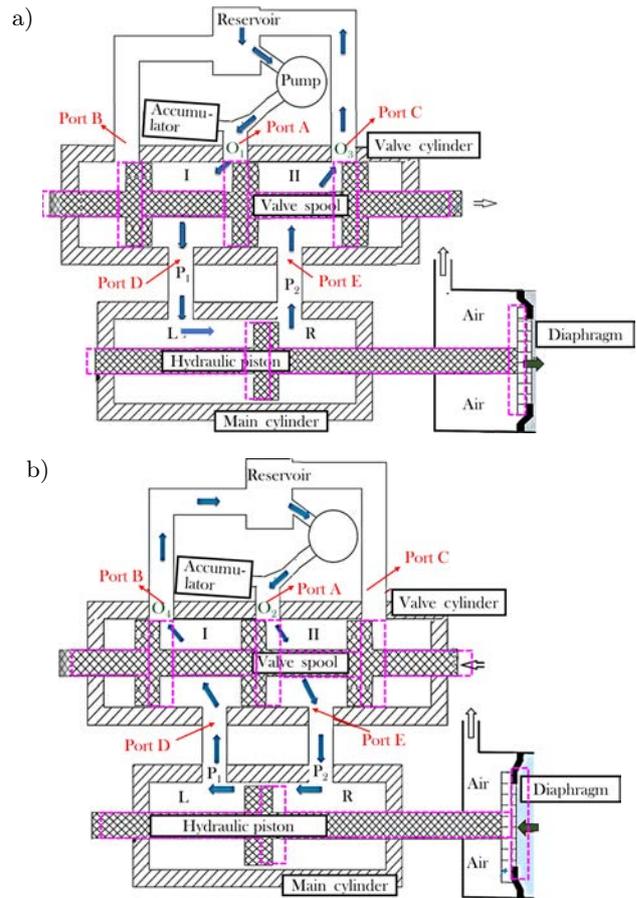
Fig. 7. Schematic of working of the device: a) spool is rightwards of neutral position, b) spool is leftwards of neutral position.

Appendix B. Experimental setup and its characterisation

To verify the mathematical model of the hydroacoustic projector, a prototype as shown in Fig. 8 was developed and tested. The projector used two-position directional control valve (Yuken DSG-03-2B2) to change the direction of flow. The mass flow rate, maximum operating pressure, and maximum operational frequency for the valve are 2 l/s, 31.5 MPa, and 2 Hz, respectively. The valve spool was actuated by an electrodynamic shaker (Data Physics GW-V20) powered by an amplifier (PA300E). The input signal to amplifier was generated from a laptop. Table 3 lists all the design parameters of the projector.

Fig. 8. Prototype of the hydroacoustic projector used in this work.

Table 3. Design parameters.

r_{cl} = 1 mm	F_f = 145 N
l_{cy} = 335 mm	V_{AC} = 750 ml
r_{cy} = 100 mm	t_p = 70 mm
r_D = 175 mm	V_f = 3%
k_D = 30 kN/m	w_v = 0.050 m
c_{air} = 340 m/s[1]	$\gamma_{air} = \gamma_{nitrogen\ gas}$ = 1.4
ρ_{air} = 1.225 kg/m^3	$\beta_{effective}$ = 25 GPa
μ_{oil} = 0.0370 Pa·s	β_{oil} = 1.48 GPa
ρ_{oil} = 805 kg/m^3	Radius of piston rod = 10 mm
Mass of piston, piston rod, diaphragm, m = 4.46 kg	
Accumulator precharge pressure = 0.3 MPa	

Figure 9 lays out the schematic of the experimental setup used in this work. Pressure sensors (Honeywell TJE 1000PSIG) were used to measure the pressure just before and after the valve. An accelerometer (Brüel & Kjær 4517) was used to measure valve accelerations. A high speed camera (Grasshopper 3 5.0 MP Mono USB3, Edmund Optics) was used to capture shaker displace images from a distance. These images were used to calculate shaker displacement using a digital image corelation software (VIC-2D, Correlated Solutions, Inc.). A laser-based motion sensor (Keyence LK-H157) was used to measure the diaphragm displacement at its
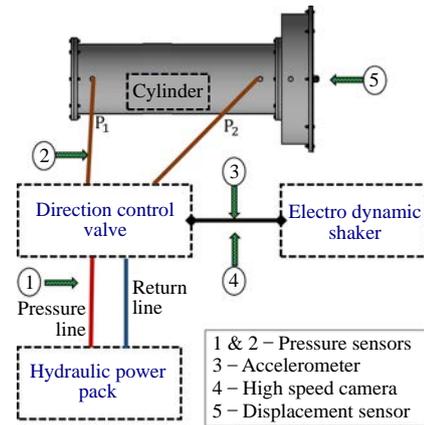
Fig. 9. Location of sensors used in the experimental setup.

centre. Data from all sensors were acquired using an NI DAQ chassis 9198 (National Instruments) with DAQ cards NI 9215 (for displacement sensor), NI 9234 (for accelerometer), and NI 9237 (for pressure sensors) at a sampling frequency of 50 kS/s (kilo samples/second).

To determine air content in oil, oil sample from an operating projector was collected and its volume was measured. Later, the entrapped air in oil was removed and the volume of oil was remeasured. In this way the amount of air entrapped in oil was determined. Also the value of $\overline{C_d}$ was calculated by measuring the instantaneous pressure drop across the valve, flow rate, and valve displacement and using these values in Eq. (12):

$$\overline{C_d} = \frac{q_{average}}{\sum(\sqrt{\Delta P_i}x_{v_i})/n} \cdot \frac{1}{w_v\sqrt{2/\rho}}. \qquad (12)$$

To estimate the value of friction between the piston and the cylinder, experiments as described in (Sreejith, Tiwari, 2020) were conducted. In these experiments the rubber diaphragm was detached from the assembly. Also a displacement sensor (Keyence LK-G5000) was used to record piston displacement, and pressure sensors (Honeywell TJE 1000PSIG) were used to record pressure inside the main cylinder. It was found that when the force on piston exceeded a threshold, it started moving. Figure 10 shows a plot of the measured friction force between piston and cylinder, as a function of piston displacement.
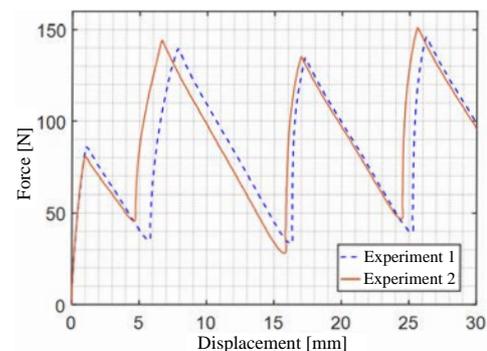
Fig. 10. Friction acting between cylinder and piston.

Acknowledgments

References

1. AKERS A., GASSMAN M., SMITH R. (2006), *Hydraulic power system analysis*, CRC Press.

2. AKKAYA A.V. (2006), Effect of bulk modulus on performance of a hydrostatic transmission control system, *Sadhana*, **31**(5): 543–556.

3. BARNWAL M., KUMAR N., KUMAR A., DAS J. (2014), Effect of hydraulic accumulator on the system parameters of an open loop transmission system, [in:] *5th International & 26th All India Manufacturing Technology, Design and Research Conference (AIMTDR 2014)*, IIT Guwahati, Assam, India, pp. 12–14.

4. BAUER B. (1954), Equivalent circuit analysis of mechano-acoustic structures, *Transactions of the IRE Professional Group on Audio*, **AU-2**(4): 112–120, doi: 10.1109/T-SP.1954.28249.

5. BERANEK L.L. (1993), *Acoustics*, American Institute of Physics, Acoustical Society of America.

6. BORUTZKY W., BARNARD B., THOMA J. (2002), An orifice flow model for laminar and turbulent conditions, *Simulation Modelling Practice and Theory*, **10**(3–4): 141–152, doi: 10.1016/S1569-190X(02)00092-8.

7. BOUYOUCOS J.V. (1987), Hydroacoustic apparatus, US Patent 4,695,987.

8. BUSCH-VISHNIAC I.J., PAYNTER H.M. (1989), Bond graph models of sound and vibration systems, *The Journal of the Acoustical Society of America*, **85**(4): 1750–1758, doi: 10.1121/1.397964.

9. CHO B.-H., LEE H.-W., OH J.-S. (2000), Estimation technique of air content in automatic transmission fluid by measurign effective bulk modulus, Technical Report, *SAE Technical Paper*.

10. DECARPIGNY J.N., HAMONIC B., WILSON O.B. (1991), The design of low frequency underwater acoustic projectors: present status and future trends, *IEEE Journal of Oceanic Engineering*, **16**(1): 107–122, doi: 10.1109/48.64890.

11. DING B., CAZZOLATO B.S., ARJOMANDI M., HARDY P., MILLS B. (2016), Sea-state based maximum power point tracking damping control of a fully submerged oscillating buoy, *Ocean Engineering*, **126**: 299–312, doi: 10.1016/j.oceaneng.2016.09.020.

12. DUBUS B., MOSBAH P., HARTMANN J.-R., GARCIN J. (2013), Ultra-low frequency underwater acoustic projectors: present status and future trends, *The Journal of the Acoustical Society of America*, **133**(5): 3266–3266, doi: 10.1121/1.4805296.

13. EDGE K., JOHNSTON D. (1991), The impedance characteristics of fluid power components: relief valves and accumulators, *Proceedings of the Institution of Mechanical Engineers, Part I: Journal of Systems and Control Engineering*, **205**(1): 11–22.

14. HEINZE A. (2008), *Modelling, simulation and control of a hydraulic crane*, M.S. Dissertation, Växjö University, School of Technology and Design.

15. IJAS M. (2007), *Damping of low frequency pressure oscillation*, Publication 656, Tampere University of Technology, http://urn.fi/URN:NBN:fi:tty-200810021110.

16. KAJASTE J.T., KAURANNE H.O., ELLMAN A.U., PIETOLA M.T. (2002), The effect of parameter uncertainty on the reliability of pressure accumulator simulations, [in:] *ASME 2002 International Mechanical Engineering Congress and Exposition*, American Society of Mechanical Engineers, pp. 75–84.

17. KARJALAINEN J.-P., KARJALAINEN R., HUHTALA K. (2012), Measuring and modelling hydraulic fluid dynamics at high pressure – accurate and simple approach, *International Journal of Fluid Power*, **13**(2): 51–59, doi: 10.1080/14399776.2012.10781053.

18. KIM W., WON D., SHIN D., CHUNG C.C. (2012), Output feedback nonlinear control for electro-hydraulic systems, *Mechatronics*, **22**(6): 766–777, Special Issue on Intelligent Mechatronics (LSMS2010 and ICSEE2010), doi: 10.1016/j.mechatronics.2012.03.008.

19. KRUS P., WEDDFELT K., PALMBERG J.-O. (1994), Fast pipeline models for simulation of hydraulic systems, *Journal of Dynamic Systems, Measurement, and Control*, **116**(1): 132–132, doi: 10.1115/1.2900667.

20. LARSON M., JÖNSSON L. (1991), Elastic properties of pipe materials during hydraulic transients, *Journal of Hydraulic Engineering*, **117**(10): 1317–1331, doi: 10.1061/(ASCE)0733-9429(1991)117:10(1317).

21. LIN K., HOLBERT K.E. (2009), Applying the equivalent pi circuit to the modeling of hydraulic pressurized lines, *Mathematics and Computers in Simulation*, **79**(7): 2064–2075, doi: 10.1016/j.matcom.2008.10.008.

22. LIU Y., DONG J., WU S., WU D., DENG Y., JI H. (2019), Theoretical research on the dynamic characteristics of electrohydraulic servo valve (EHSV) in deep sea environment, *Ocean Engineering*, **192**: 105957, doi: 10.1016/j.oceaneng.2019.04.038.

23. MATKO D., GEIGER G., GREGORITZA W. (2000), Pipeline simulation techniques, *Mathematics and Computers in Simulation*, **52**(3–4): 211–230, doi: 10.1016/S0378-4754(00)00152-X.

24. MATLAB (n.d.), *Matlab simscape fluids*, last accessed June 07, 2020, https://in.mathworks.com/products/simscape-fluids.html.

25. MERRITT H.E. (1967), *Hydraulic control systems*, John Wiley & Sons.

26. MIKOTA G. (2013), Modal analysis of hydraulic pipelines, *Journal of Sound and Vibration*, **332**(16): 3794–3805, doi: 10.1016/j.jsv.2013.02.021.

27. PAN X., WANG G., LU Z. (2011), Flow field simulation and a flow model of servo-valve spool valve orifice, *Energy Conversion and Management*, **52**(10): 3249–3256, doi: 10.1016/j.enconman.2011.05.010.

28. PEÑA O.R., LEAMY M.J. (2015), An efficient architecture for energy recovery in hydraulic elevators, *International Journal of Fluid Power*, **16**(2): 83–98, doi: 10.1080/14399776.2015.1055991.

29. RUAN J., BURTON R. (2006), Bulk modulus of air content oil in a hydraulic cylinder, [in:] *ASME 2006 international mechanical engineering congress and exposition*, American Society of Mechanical Engineers, pp. 259–269.

30. SCHÖNFELD J. (1954), Analogy of hydraulic, mechanical, acoustic and electric systems, *Applied Scientific Research*, Section B, **3**(1): 417–450.

31. SMITH B. (1994), The modelling of underwater, electroacoustic, sonar transducers, *Applied Acoustics*, **41**(4): 337–363, Special Issue on Transducers, doi: 10.1016/0003-682X(94)90093-0.

32. SREEJITH V.S., TIWARI N. (2016a), Modelling and simulation of a hydro-acoustic projector, [in:] *The 23rd International Congress on Sound and Vibration*, pp. 4392–4399, International Institute of Acoustics and Vibration (IIAV), Athens, Greece, http://www.scopus.com/inward/record.url?eid=2-s2.0-84987850929&partnerID=MN8TOARS.

33. SREEJITH V.S., TIWARI N. (2016b), Development and simulation of an electrically analogous model for an electro-hydro-acoustic projector, *International Symposium on Acoustics for Engineering Applications NSA*, Gurugram, India.

34. SREEJITH V.S., TIWARI N. (2020), Modelling of a hydroacoustic projector to produce low frequency sound, *The Journal of the Acoustical Society of America*, **147**(4): 2682–2693, doi: 10.1121/10.0001133.

35. SREEJITH V.S., TIWARI N. (2021), Influence of compliance, and effective orifice discharge coefficient on performance of a hydroacoustic projector, *Applied Acoustics*, **177**: 107921, doi: 10.1016/j.apacoust.2021.107921.

36. SUI H., LU X. (2018), Nonlinear dynamic analysis of complex hydraulic driving processes, *Journal of Sound and Vibration*, **430**: 115–133, doi: 10.1016/j.jsv.2018.05.034.

37. TOTTEN G.E. (2011), *Handbook of Hydraulic Fluid Technology*, CRC Press.

38. WU D., BURTON R., SCHOENAU G., BITNER D. (2003), Modelling of orifice flow rate at very small openings, *International Journal of Fluid Power*, **4**(1): 31–39, doi: 10.1080/14399776.2003.10781153.

39. YANG H., FENG B., GONG G. (2011), Measurement of effective fluid bulk modulus in hydraulic system, *Journal of Dynamic Systems, Measurement, and Control*, **133**(6): 061021, doi: 10.1115/1.4004783.